Hypoxia suppresses myofibroblast differentiation by changing RhoA activity

Running title: ArhGAP29 in response to hypoxia

Lisa Leinhos[1], Johannes Peters[1], Sabine Krull[1], Lena Helbig[1], Melanie Vogler[1], Magdolna Levay[2], Gijsbert J. van Belle[1], Anne J. Ridley[3, 4], Susanne Lutz[5], Dörthe M. Katschinski[1], Anke Zieseniss[1]

[1] Institute of Cardiovascular Physiology, University Medical Center, Georg-August University, Göttingen, 37073 Göttingen, Germany

[2] Experimental Pharmacology, European Center of Angioscience, Medical Faculty Mannheim, Heidelberg University, 68167 Mannheim, Germany

[3] Randall Centre of Cell and Molecular Biophysics, King's College London, London SE1 1UL, UK

[4] School of Cellular and Molecular Medicine, University of Bristol, Bristol BS8 1TD, UK

[5] Institute of Pharmacology and Toxicology, University Medical Center, Georg-August University Göttingen, 37075 Göttingen, Germany

* Author for correspondence: anke.zieseniss@med.uni-goettingen.de

Key words: hypoxia, RhoA; MRTF-A, myofibroblast, hypoxia-inducible-factor, ArhGAP29

Summary statement

We show that hypoxia impairs myofibroblast differentiation, and link the HIF-signaling pathway to MRTF-A signaling via ArhGAP29.

Abstract

Fibroblasts show a high range of phenotypic plasticity including the transdifferentiating into myofibroblasts. Myofibroblasts are responsible for the generation of the contraction forces that are important for wound healing and scar formation. Overactive myofibroblasts on the other hand are involved in abnormal scarring. Cell stretching and extracellular signals such as transforming growth factor β can induce the myofibroblastic program whereas microenvironmental conditions such as reduced tissue oxygenation have an inhibitory effect. We investigated the effects of hypoxia on myofibroblastic properties and linked this to RhoA activity. Hypoxia reversed the myofibroblastic phenotype of primary fibroblasts. This was accompanied by decreased αSMA expression, alterations in cell contractility, actin reorganization, and RhoA activity. We identified a hypoxia-inducible induction of ArhGAP29, which is critically involved in MRTF-A (myocardin-related transcription factor-A) signaling, the differentiation state of myofibroblasts and modulates RhoA activity. This novel link between hypoxia and MRTF-A signaling is likely to be important for ischemia-induced tissue remodeling and the fibrotic response.

Introduction

Fibroblasts are critical for wound healing and repair. Activation of fibroblasts results in deposition of extracellular matrix (ECM) into the surrounding tissue. Fibroblasts are highly plastic and show a range of phenotypes upon stimulation, including the differentiation of fibroblasts into myofibroblasts. Myofibroblasts are not terminally differentiated cells as they can revert back to fibroblasts. This de-differentiation has been described in several tissues, however, the precise molecular mechanism has just begun to be explored in detail (Jun and Lau, 2018). Myofibroblasts are important players in regulating connective tissue remodeling by combining ECM synthesis with characteristics of smooth muscle cells. Myofibroblasts are responsible for the generation of the contraction forces that are important for tissue healing. Overactive myofibroblasts on the other hand are involved in organ fibrosis and abnormal scarring causing detrimental tissue deformation and dysfunction (Hinz et al., 2012; Tomasek et al., 2002a). A fundamental initiator of myofibroblast differentiation is the cytokine transforming growth factor β (TGF-β), which is part of a cytokine milieu that is generated within an injury environment. Cultivated primary fibroblasts retain fibroblast markers only in early passages but with increased time after plating on the stiff surface of a culture dish they begin to transdifferentiate spontaneously into myofibroblasts even without addition of TGF-β. Thus, there are clearly other molecular regulators in play, including the actin cytoskeleton stress sensing through the GTPase RhoA and its downstream effectors, which act to sense changes in the microenvironment. For example, stimuli like stiffness or stretch and oxygenation are important triggers of the myofibroblastic program (Sen and Roy, 2010; Wynn and Ramalingam, 2012).

In the biomedical context, tissue oxygenation is important since wound or tissue healing mostly takes place under reduced oxygen availability, and indeed hypoxia has been reported to inhibit myofibroblast differentiation (Madsen et al., 2015; Modarressi et al., 2010). However, it is largely unknown how tissue oxygenation affects the molecular events underlying this process including the regulation of Rho-GTPase activities. Rho-GTPases are essential players in the control of fibroblast properties (Kis et al., 2011). Nonetheless, details of the molecular mechanisms whereby Rho-signaling is altered in hypoxia and the connection to Hypoxia inducible factor (HIF), the transcriptional master regulator of the cellular hypoxic response, are poorly understood. HIF is a heterodimeric transcriptional complex consisting of an α- and a β-subunit. The activity of HIF is controlled by oxygen dependent prolyl hydroxylation catalyzed by the three HIF prolyl-4-hydroxylase domain enzymes (PHD 1-3) (Epstein et al., 2001; Ivan et al., 2001; Jaakkola et al., 2001). Hydroxylation of the HIFα subunit renders it prone for subsequent ubiquitination by the von Hippel-Lindau (VHL) protein complex and proteasomal degradation. In hypoxia HIF accumulates and activates the expression of a multitude of target genes, including genes involved in cell growth and metabolism (Bishop and Ratcliffe, 2014).

In mammals, the Rho family of GTPases consists of 20 members (Hall, 2005) with Cdc42, Rac1 and RhoA being the best characterized family members. RhoA promotes the formation of integrin-mediated focal adhesions and actin stress-fibers and modulates myofibroblast differentiation via MRTF-

A (myocardin-related transcription factor-A) signaling (O'Connor and Chen, 2013). Rho GTPases are in general active when bound to GTP and inactive when bound to GDP. The switch from the GDP-bound state to the GTP-bound state is mediated by GEFs (guanine-nucleotide exchange factors). GAPs (GTPase-activating proteins), on the other hand, inactivate Rho GTPases (Hodge and Ridley, 2016; Ridley, 2006). RhoA has been reported to be activated in hypoxia in a variety of cell types including tumor cells (Gilkes et al., 2014), pulmonary endothelial cells (Wojciak-Stothard et al., 2005), pulmonary artery smooth muscle cells (Bailly et al., 2004), and ventricular myocytes (Gonzalez-Rodriguez et al., 2015). Nonetheless there are also opposite reports showing no change or even a decrease in RhoA activity in hypoxia (Bailly et al., 2004; Fediuk et al., 2012; Raheja et al., 2011; Zieseniss, 2014). In most of these studies however, RhoA activity was studied just at one time point after the onset of hypoxia and was not related to the myofibroblastic program.

We set out to investigate the effects of hypoxia on myofibroblastic properties and showed that hypoxia results in decreased RhoA activity and loss of αSMA-positive primary fibroblasts. We identified a new regulatory mechanism underlying the inhibition of myofibroblast differentiation in hypoxia, whereby the hypoxia-inducible expression of ArhGAP29 effects the fibrosis associated MRTF-A and contributes to the modulation of RhoA activity.

Results

Hypoxia reverts myofibroblastic phenotype in primary skin fibroblasts

During their maturation myofibroblasts express α-smooth muscle actin (αSMA), which is responsible for wound contraction. αSMA discriminates myofibroblasts from fibroblasts and has become the most frequently used marker for this cell type. After plating, primary fibroblasts spontaneously undergo myofibroblast differentiation and express αSMA incrementally over time (Goffin et al., 2006). Consistent with this, we observed increased αSMA mRNA levels 24-48 h after plating of primary skin fibroblasts (Fig. 1A). To confirm that hypoxia affects this fibroblast-to-myofibroblast differentiation program, primary skin fibroblasts were then exposed to hypoxic conditions (1% O_2 for 4 and 24 h). In hypoxia αSMA mRNA expression decreased significantly. Also transgelin (TAGLN) mRNA expression, which is another myofibroblast marker, decreased in hypoxia (Fig. 1A). These changes in myofibroblast differentiation were further supported by immunofluorescence staining (Fig. 1B and C). The number of positive cells in which αSMA colocalizes with F-actin decreased significantly when cells were cultivated in hypoxic conditions for 24 or 48 h. Addition of TGF-β to primary fibroblasts in normoxia increased αSMA and TGLN mRNA levels. This response was likewise reduced in hypoxia (Fig. 1D). αSMA is responsible for the generation of contractile force in myofibroblasts (Hinz et al., 2002), and thus the ability to contract collagen matrices is another characteristic of myofibroblast differentiation (Bochaton-Piallat et al., 2016; Tomasek et al., 2002b). Fibroblasts were therefore cultured in a polymerized collagen matrix in normoxia or hypoxia for 24 h (Fig. 1E), then the matrices were released from the culture dish resulting in mechanical unloading and contraction driven by the force generated by the cells. Consistent with the decreased expression of αSMA in hypoxia, the contraction of the collagen matrices by fibroblasts in low oxygen concentration was significantly lower compared to the normoxic conditions. As a positive control for loss of cell-driven collagen contraction, some culture dishes were treated with the myosin ATPase inhibitor 2, 3-BDM (Fig. 1E). These dishes showed a clearly reduced collagen contraction compared to untreated collagen matrices.

In addition to αSMA expression, myofibroblasts are characterized by the presence of actin stress fibers. We compared the F-actin structures in the primary fibroblasts in normoxia and hypoxia (Fig. 2A). Whereas in normoxia the αSMA-positive cells showed prominent actin filaments traversing almost the entire cell, in hypoxia (in non αSMA-positive cells) actin filaments were shorter and located closer to the cell periphery. We quantified this actin filament modulation by applying a non-biased cluster analysis and verified that the structural patterns indeed change significantly between the two conditions (Fig. 2B).

The Rho GTPase RhoA is known to promote stress fiber formation during myofibroblast differentiation (Small, 2012). Indeed, inhibiting Rho GTPases under normoxic conditions by adding C3 transferase, a known inhibitor of RhoA, RhoB and RhoC signaling (Vogelsgesang et al., 2007), reduced the number of αSMA-positive cells in normoxia (Fig. 2C and D). This effect was similar to the decrease observed

in hypoxia which led us to speculate that altered RhoA signaling is involved in the hypoxia-mediated depression of the myofibroblastic phenotype. Of note, treating the fibroblasts with C3 transferase in hypoxia resulted in increased cell toxicity, which precluded analysis of αSMA expression in these conditions. We then investigated the effect of hypoxia on RhoA activity (Fig. 2E). Correlating with the reduced myofibroblastic phenotype, RhoA activity decreased after 24 h of hypoxic exposure following a transient increase in RhoA activity at 4 - 12 h of hypoxia.. To gain mechanistic insight into how RhoA activity is regulated in hypoxia, we chose to use two cell lines in which we could screen for Rho regulators, L929 cells and SV40-immortalized and transformed mouse embryonic fibroblasts (MEFs). L929 cells were originally derived from normal subcutaneous areolar mouse tissue and show some fibroblastic features, e. g. a typical fibroblast-like architecture, like the MEFs. Similar to the primary fibroblasts, 24 h of hypoxia resulted in a reduction in RhoA activity in both cell lines that coincided with the increase in HIF-1α protein levels. (Fig. 2 F, G). However, the kinetics of RhoA activity changes were slightly different in the cell lines with the transient maximum RhoA activity increase shifted to earlier time points, i.e. RhoA activity was increased already after 30 min of hypoxia and declined after 4 and 24 h. Since the L929 and the MEF cells showed a similar pattern of RhoA activation in hypoxia we used them as model systems to investigate how RhoA is regulated in response to hypoxia.

The expression of the GTPase activating protein ArhGAP29 is induced by hypoxia

To determine how RhoA activity is altered by hypoxia, we investigated the expression of the two major classes of regulatory proteins that affect the activation state of RhoA: GEFs that activate RhoA by promoting exchange of GDP for GTP, and GAPs that enhance the intrinsic GTP-hydrolysis activity leading to RhoA inactivation. We determined the effect of hypoxia on the mRNA expression of a panel of GEFs and GAPs in L929 cells for which activity towards RhoA had been reported (Fig. 3A). Among the GEFs and GAPs analyzed, we found several that were significantly downregulated in hypoxic conditions (e.g. ArhGAP5, ArhGAP18, ArhGAP19, OPHN1, ArhGEF1, ArhGEF15, Net1, and Trio). However, only two upregulated mRNAs were identified (e.g. ArhGAP29 and ArhGAP35), the most prominent being ArhGAP29. ArhGAP29 mRNA was already induced at 1 h and peaked at about 4 h after the onset of hypoxia (Fig. 3B). Rapid accumulation of the HIF-1α protein was detectable after 1 h (Fig. 3C), suggesting that ArhGAP29 could be induced downstream of HIF-1.

We investigated this possibility by treating cells with DMOG, a pharmacological inhibitor of the PHDs that results in the stabilization of HIF-1α independent of the oxygen concentration (Jaakkola et al., 2001). DMOG is therefore commonly used as a hypoxia mimetic agent. Similar to the effects observed in hypoxia, treatment of L929 cells with DMOG for 24 h induced ArhGAP29 mRNA (Fig. 3D) and protein (Fig. 3E) levels. The induction of ArhGAP29 in hypoxia was also observed in other cell lines (murine C2C12 and MEF) and primary mouse cardiac (PCF) and skin fibroblasts (PSF) (Fig. 3F), indicating that it is generally induced by hypoxia.

ArhGAP29 induction in hypoxia is HIF-1α dependent

To elucidate whether the hypoxia-inducible ArhGAP29 expression requires the HIF pathway, two independent, stable HIF-1α knockdown L929 cell clones (c1 and c2) were used. ArhGAP29 (Fig. 4A) and PHD3 mRNA (Fig. 4B) levels were analyzed. PHD3 is a well-studied HIF target gene (Marxsen et al., 2004). The hypoxic induction of both PHD3 and ArhGAP29 mRNA was significantly reduced in the HIF-1α knockdown cells compared to non-transduced control and the non-targeting sh-control (shC) cells. In agreement with these observations, no obvious increase in ArhGAP29 protein levels was observed in response to hypoxia in these cells (Fig. 4C). To further analyze the role of HIF-1 in the hypoxic induction of ArhGAP29, we used MEF cells that were originally isolated from HIF-1α knockout embryos (Ryan et al., 2000). As expected PHD3 induction was blunted in the MEF HIF-1α knockout cells (MEF -/-) compared to the control MEF (MEF +/+) cells in hypoxia (Fig. 4D). ArhGAP29 mRNA (Fig. 4E) and protein (Fig. 4F) levels were likewise reduced in MEF-/- cells when compared to MEF +/+ cells. Together these results underline the importance of HIF-1α for the induction of ArhGAP29 in hypoxia.

Depletion of ArhGAP29 affects RhoA activity, actin filament organization, and nuclear accumulation of MRTF-A

To determine the role of hypoxia-induced ArhGAP29 expression, ArhGAP29-depleted L929 cells were established. A successful knockdown of ArhGAP29 was confirmed at the mRNA and protein level (Fig. 5A and B). In line with its GAP function, ArhGAP29 has been described to negatively regulate RhoA activity in endothelial cells (Post et al., 2013). ArhGAP29-depleted L929 cells similarly had increased RhoA activity in normoxia (Fig. 5C and Fig. S1A). In the L929 control cells, RhoA activity was decreased 24 h after onset of hypoxia. Although in principle the trend was similar in the ArhGAP29 knockdown cells, the kinetics of RhoA activity was skewed with an overall longer significantly increased RhoA activity. Whereas 4 h after onset of hypoxia RhoA activity was already significantly decreased in the control cells, the activity of RhoA was still at higher levels in the ArhGAP29 knockdown cells (Fig. 5D and Fig. S1B).

As described above, RhoA promotes the formation of actin filaments. We therefore investigated the contribution of ArhGAP29 to F-actin organization using non-biased cluster analysis. In L929 ArhGAP29 knockdown cells F-actin structures were significantly changed compared to control cells (Fig. S2).

RhoA is well known to regulate the transcription factors serum response factor (SRF) and the myocardin-related family of transcriptional coactivators A (MRTF-A) and B (MRTF-B), which are also central to the induction of the myofibroblastic program (Small, 2012). SRF regulates gene expression via binding to specific serum response elements (SRE). Specificity of target gene activation by SRF is accomplished via interactions with transcriptional co-regulators including MRTF-A and MRTF-B. MRTFs are inhibited by monomeric actin, and activated when actin is polymerized (Olson and Nordheim, 2010). The observed increase in RhoA activity in concert with enhanced F-actin formation

196 in the ArhGAP29-depleted cells led us to investigate MRTF-A localization in normoxia and hypoxia
197 (Fig. 6A, B). ArhGAP29 knockdown enhanced the nuclear localization of MRTF-A in both normoxic
198 and hypoxic conditions. To analyze whether the increased nuclear accumulation of MRTF-A in
199 ArhGAP29 knockdown cells indeed requires functional Rho, cells were treated with C3 transferase.
200 Upon C3 transferase treatment MRTF-A remained more cytoplasmic in hypoxic control cells as well as
201 ArhGAP29 knockdown cells. Similar results were obtained when we analyzed the localization of ectopic
202 MRTF-A-GFP. Like endogenous MRTF-A, MRTF-A-GFP showed increased nuclear localization in
203 ArhGAP29-depleted cells compared to control fibroblasts (Fig. 6C, D). This led to increased SRF
204 activity, as indicated by an increased activity of a SRE-driven luciferase reporter-plasmid (Fig. 6E) and
205 increased mRNA expression of the SRF/MRTF target gene CTGF (Fig. 6F) in the ArhGAP29
206 knockdown cells compared to the control cells.

207 **Knockdown of ArhGAP29 prevents the hypoxia-induced reversal of myofibroblast differentiation**
208 Although L929 and MEF cells have some fibroblastic features, they are not able to differentiate into
209 myofibroblasts. Having established that ArhGAP29 is inducible in hypoxia and affects one major
210 myofibroblastic pathway, we used the primary mouse skin fibroblasts to analyze the influence of
211 ArhGAP29 on myofibroblast differentiation in hypoxia. To this end we transduced primary skin
212 fibroblasts with a plasmid expressing either a non-targeting shRNA (shC) or a shRNA targeting
213 ArhGAP29 via lentiviral transduction. The knockdown efficiency of ArhGAP29 in normoxia and
214 hypoxia was verified by qRT-PCR (Fig. S3). In normoxia as well as hypoxia, the knockdown of
215 ArhGAP29 was accompanied by higher αSMA mRNA levels compared to the respective controls (Fig.
216 7A). As described above αSMA and levels were reduced in hypoxia. The same effect was observed in
217 the non-targeting shRNA transduced cells. In the ArhGAP29 knockdown cells, however, hypoxia no
218 longer decreased the expression of αSMA. We also observed a higher number of αSMA-positive
219 ArhGAP29 knockdown cells compared to control and shC fibroblasts in normoxia and hypoxia (Fig.
220 7B), indicating that the knockdown of ArhGAP29 prevented the effects of hypoxia on the
221 myofibroblastic program.

Discussion

Fibroblast activation and ECM production are necessary during tissue healing, but severe or repetitive tissue injury can lead to a progressive irreversible fibrosis that might eventually result in organ malfunction (Wynn, 2008). Contractility of fibroblasts at the wound site is important for physiological and pathological wound healing. Therefore, transdifferentiation of fibroblasts into contractile myofibroblasts is an essential regulatory step in fibrosis (Bochaton-Piallat et al., 2016). This process requires a highly orchestrated signaling network involving RhoA signaling (Small, 2012). We show here that one key microenvironmental condition, hypoxia, influences the myofibroblastic program. Hypoxia in wounds is the result of reduced capillary density within the injured tissue and increased oxygen consumption during wound healing. As a result, fibrotic tissue stabilizes the transcription factor HIF-1α (Hong et al., 2014). In line, preclinical studies show that initiation and progression of tissue fibrosis are closely correlated with HIF-1α and hypoxia-induced, pro-fibrotic genes (Botusan et al., 2008; Kimura et al., 2008). This places the HIF system in the center of interest for the development of novel therapies in fibrosis (Xiong and Liu, 2017). Hypoxia is widely known to also regulate other important steps in the remodeling phase of wound healing including innate immune function and epithelial-mesenchymal transition (EMT) (Scheid et al., 2002; Wottawa et al., 2013; Yang et al., 2008). In sharp contrast, the consequences of hypoxia for the transdifferentiation of fibroblasts into myofibroblasts as well as the reversion of this process are less understood. In the presented data, we demonstrate that hypoxia indeed affects the myofibroblastic programme. We cannot formally prove that the myofibroblastic programme is reversed instead of a depression of the transdifferentiation of fibroblasts to myofibroblast. The kinetics of the expression of αSMA following exposure to hypoxia, however strongly indicate that the myofibroblastic programme, that is initiated by the mechanical stimulus upon seeding the cells on the stiff plastic surface is reverted. We identified in this study that the expression of ArhGAP29, which is an important regulator of RhoA activity, is highly depending on the oxygenation. The promoter region of ArhGAP29 contains several hypoxia response elements (HREs), which are putative HIF-1 binding sites. Whether these are functional and if ArhGAP29 is a direct or indirect HIF-1 target gene remains to be analyzed.

Mutations within the coding exons of ArhGAP29 have been associated with nonsyndromic cleft lip with or without cleft palate birth defects (Butali et al., 2014; Chandrasekharan and Ramanathan, 2014; Leslie et al., 2016; Liu et al., 2017a; Liu et al., 2017b; Savastano et al., 2017). Mice with reduced ArhGAP29 protein expression levels die perinatally with signs of abnormal cranofacial, limb and skin morphogenesis (Biggs et al., 2014, Ingraham et al., 2006) and a ArhGAP29 knockout in epiblast cells results in embryonic death at midgestation (Barry et al., 2016). Furthermore, reduced expression of ArhGAP29 has been correlated with cancer metastasis (Qiao et al., 2017) and endometrial fibrosis (Xu et al., 2017). These data indicate that ArhGAP29 levels need to be tightly controlled to ensure for accurate embryonic development. Our study underpins the assumption that a close regulation of

ArhGAP29 expression levels is important for proper cell function in normoxia and shows for the first time a role for ArhGAP29 in hypoxia.

A knockdown of ArhGAP29 in our cell models resulted in increased RhoA activity accompanied by changes in cell morphology and enhanced actin filament formation under normoxic and hypoxic conditions (Fig. 7C). The rearrangement of the actin cytoskeleton is known to liberate MRTF-A from G-actin and thereby, in concert with SRF, to modulate gene expression (Olson and Nordheim, 2010). Hence, the increase in nuclear MRTF-A localization in ArhGAP29 knockdown cells can most likely be attributed to an increase in RhoA activity especially as the increased nuclear localization of MRTF-A in the knockdown cells was reversible by treatment with the Rho-inhibitor C3 transferase. The increase of RhoA activity and rearrangement of actin filaments seen in ArhGAP29 knockdown cells in our study however most likely influences not only cell morphology and MRTF-A mediated gene expression but also other actin-linked cellular functions like cell motility. The MRTF-SRF signaling axis is activated in response to skin injury but is also part of fibrosis-associated pathologies for example in the ischemic heart (Small, 2012; Velasquez et al., 2013). Increasing MRTF-A activation by small molecules has been shown to support skin wound healing (Velasquez et al., 2013). Deletion of MRTF-A in mice on the other hand attenuates myofibroblast responses and reduces cardiac fibrosis and scarring following ischemia (Small et al., 2010). Thus, targeting MRTF could be a useful strategy in treating diseases associated with inappropriate myofibroblast activity. Having discovered a role of ArhGAP29 for MRTF-A activation and myofibroblast differentiation in hypoxia may prove to be useful in this regard. The knockdown of ArhGAP29 results in higher basal RhoA activity and more prolonged RhoA activity in hypoxia. We cannot exclude the possibility that the increase in basal RhoA activity accounts for the observed change in RhoA activity kinetics. As the knockdown of ArhGAP29 does not completely prevent the decrease in RhoA activity, it is likely that other GAPs in addition to ArhGAP29 are involved in regulating RhoA activity in hypoxia. There are indeed around 69 putative RhoGEFs belonging to the Dbl-family (DH-PH sequence), roughly 24 of those are clearly associated with RhoA activity (Rossman et al., 2005) Regarding RhoGAPs, around 66 human variants are described, however the association to RhoA activity of some of those is unclear and not well defined (Amin et al., 2016). Considering this complex network with many players involved, it is anticipated that ArhGAP29 is not the sole player involved in the hypoxic regulation of RhoA activity. Although there is limited evidence that specific small molecule modulators of GAPs can be developed (Dang et al., 2017), the regulation of ArhGAP29 by the HIF pathway may be useful for a targeted approach. Notably, the HIF system can be activated by small molecule inhibitors of the PHD enzymes (Katschinski, 2009). Treating cells with DMOG, which is a competitive inhibitor of oxoglutarate binding to the PHDs, indeed proved that manipulating the HIF system also affects ArhGAP29 expression.

Taken together, the hypoxia-dependent ArhGAP29 expression reverses myofibroblast differentiation via the SRF/MRTF signaling pathway, and modulates RhoA activity. RhoA is primarily associated with cytoskeletal regulation, including actin stress fiber formation and actomyosin contractility as

295 demonstrated here. The link we have identified between hypoxia, ArhGAP29 and the myofibroblastic
296 phenotype provides new insight into how limited oxygen availability acts at a molecular level leading
297 to cell differentiation.

Materials and Methods

Chemicals

Dimethyloxalylglycine (DMOG) and TGF-β were purchased from Enzo Life Sciences and PreproTEch, respectively. If not indicated otherwise all other chemicals were purchased from Sigma (Sigma-Aldrich, Munich, Germany).

Cell Culture

C2C12, L929 and MEF cells were cultivated in high glucose modified Eagles medium (Pan, Biotech, Aidenbach, Germany) supplemented with 10% fetal calf serum (Biochrom, Berlin, Germany), 50 units/ml penicillin, and 50 µg/ml streptomycin (Pan Biotech). C2C12 and L929 cells were obtained from S. Rohrbach (Institute of Physiology, Justus Liebig University Giessen, Germany) and ATCC respectively. MEF HIF-1α+/+ and MEF HIF-1α−/− cells were a kind gift of R.S. Johnson (Department of Physiology, University of Cambridge, UH.). Cells were tested regularly for mycoplasma with DAPI. For isolating primary skin fibroblasts, mouse tails were sterilized and digested over night with collagenase II (Biochrom, Berlin, Germany) dissolved in culture medium. Cells were dislodged from digested tails by filtering the cells through a 70 µm netting and subsequently cultured in DMEM/F12 media supplemented with 1% non-essential amino acids, 10% fetal calf serum, 50 units/ml penicillin, and 50 µg/ml streptomycin. Primary cardiac fibroblasts were isolated from finely minced mouse heart tissue. Tissue was digested under constant agitation in Hank´s buffered salt solution supplemented with 100 U/ml collagenase (Biochrom, Berlin, Germany) and 0.1% Trypsin. The digestion buffer was replaced 5 times. The dispersed cells were incubated on a cell culture dish in DMEM/F12-Glutamax supplemented with 10% fetal calf serum, 100 µM ascorbic acid, 50 units/ml penicillin and 50 µg/ml streptomycin. The culture medium was replaced after 2 h to remove non-attached non-fibroblasts.

L929 ArhGAP29 knockdown clones and primary skin fibroblasts ArhGAP29 knockdown cells were generated by lentiviral transduction with pLKO.1-puro ArhGAP29-shRNA expression vectors (TRCN0000023926, Sigma-Aldrich, St. Louis, USA). For generating the shControl (shC) transfected cells, a pLKO.1-puro vector was used containing a non-targeting shRNA (#SHC002, Sigma-Aldrich) (Vogler et al., 2013).

Viral particles were produced in HEK293T cells using the ViraPower lentiviral expression kit according to the manufacturer's instructions (Life Technologies, Carlsbad, California, USA). 20 µg/ml puromycin (Life Technologies) were used to select for L929 cells with successfully integrated plasmid; 7 µg/ml puromycin were used for selection of primary skin fibroblasts.

For hypoxic conditions, O_2 levels were decreased to 1% O_2 with N_2 in an *in vivo 400* work station (Baker Ruskinn, Sanford, Maine, USA).

Where indicated cells were treated with C3 Transferase (Cytoskeleton, Inc.). L929 cells were treated with 2 µg/ml, primary fibroblasts were incubated with 0.7 µg/ml C3 transferase.

Transfection

Transfections were performed using Lipofectamine (Thermo Fisher Scientific) according to the manufacturer's instructions. The MRTF-A-GFP vector was a gift from Guido Posern, Martin-Luther University Halle-Wittenberg, Germany. MRTF-A GFP localization was quantified using ImageJ. The GFP intensity of an area within the nucleus and an area within the cytoplasm within the same cell were measured. The ratio nuclear/cytoplasmic intensity was calculated.

Immunofluorescence

For immunofluorescence staining, cells were fixed with 4% paraformaldehyde for 15 min. Subsequently, cells were washed with PBS and incubated with 0.1% Triton X-100 for 15 min. 5% BSA in PBS was used as a blocking solution. For detection of αSMA the 1A4 anti-αSMA antibody (1:500, A2547, Sigma-Aldrich) was used. The anti-MRTF-A antibody (1:200) was a kind gift from Guido Posern (Institute for Physiological Chemistry Martin Luther University Halle-Wittenberg, Germany). Quantification of endogenous MRTF-A was performed as described above for MRTF-A GFP. After incubation with primary antibodies (1 h at room temperature) cells were washed three times with PBS, and secondary antibodies (anti-mouse FITC (1:100, F0257), anti-mouse Alexa fluor 594 (1:1000,Thermo Fisher Scientific, A11032), anti-rabbit FITC 488 (1:200, F0382)) were added for 1 h at room temperature. For F-actin labeling fixed cells were incubated with Alexa Fluor® 594 Phalloidin (1:400,Thermo Fisher Scientfic) or Texas-red Phalloidin (1:400, Invitrogen, Darmstadt, Germany) for 20 min in the dark. Nuclei were counterstained with DAPI. Coverslips were mounted with Fluoromount™ and analyzed using either an inverted fluorescence microscope IX83 (Olympus), an Axiovert 200 M fluorescence microscope (Zeiss) with a 63× Plan-Neofluar 1.3 NA water-corrected objective and appropriate filter settings, or an LSM 510-META confocal laser scanning microscope (Zeiss) and processed using ImageJ and Adobe Photoshop CS2.

Quantification of actin clusters

For F-actin cluster analysis pictures of Alexa Fluor 594-conjugated phalloidin stained cells were analyzed using the *Actin Analyzer 2D* plugin (http://www2.informatik.uni-halle.de/agprbio/mitobo/index.php/Applications/ ActinAnalyzer2D) from the extension package MiToBo in ImageJ (Möller et al., 2016). This tool allows to discern, characterize, and extract local structural patterns occurring within the actin cytoskeleton of phalloidin stained cells. Gray-level co-occurrence matrices are first calculated to generate statistics over the existence of specific pairs of pixels in a local region of interest or tile. From these matrices, 10 customary texture features (including but not limited to: entropy, contrast, cluster shade, and autocorrelation) are calculated in 4 different directions. All these vectors are then concatenated to form a 40 dimensional feature vector of each tile. Each of the tiles belonging to a cell is clustered for structural pattern discovery between images and cells. The resulting pseudo-colored images show areas within cells that have similar local structural patterns in the actin cytoskeleton. The area a pseudo-coloring covers can be measured and is represented in a bar graph

representing the percentage of area of the cells having a certain local structural pattern in the actin cytoskeleton.

Collagen Contraction assay

The collagen contraction assays were performed according to the manufacturer´s protocol (Cell Biolabs, CBA-201, San Diego, CA). In brief, a primary skin fibroblast cell suspension of 5 x 10^6 cells/mL was obtained. 100 µl of this cell suspension were mixed with 400 µl collagen gel working solution and added to one well of a 24-well plate. Medium was added after one hour. Cultures were incubated for 1 day followed for another 24 h of either hypoxic (1% O_2) or normoxic (20% O_2) incubation. 30 min before releasing the stressed matrix with a sterile spatula, control wells were treated with the contraction inhibitor 2, 3-Butanedione Monoxime (BDM).

Luciferase reporter gene assay

L929 cells were transfected with the firefly luciferase (FL) reporter construct pSRE.L (a gift from Dr J. Mao and Dr D. Wu, University of Rochester, Rochester, NY, USA), encoding the FL under the control of a modified serum response transcriptional regulatory element, referred to as SRE.L (Mao et al., 1998). Transfections were carried out with Lipofectamine 2000 (Invitrogen) according to manufacturer´s guidelines and were normalized by cotransfecting the Renilla luciferase (RL) control plasmid pRL.TK (Promega, Mannheim, Germany). pSRE.L and pRL.TK were transfected at a 1:1000 ratio. Cells were placed into hypoxic (1% O_2) conditions 24 hours after transfection; in addition respective controls were kept under normoxic (20% O_2) conditions. Cells were lysed 48 hours after transfection. Activities of FL and RL were measured by using the Dual-Luciferase Reporter Assay System (Promega).

RNA isolation and qRT PCR

For RNA isolation cells were briefly washed with PBS and harvested in Trizol (Invitrogen, Darmstadt, Germany). RNA was isolated according to the manufacturer's instructions. 1 µg of RNA was transcribed using the First Strand cDNA Synthesis Kit (Fermentas, St. Leon-Rot, Germany) according to manufacturer's instruction. Transcript levels were analyzed by quantitative real-time PCR (qRT-PCR) amplifying 1 µL of cDNA with Brilliant II SYBR Green qPCR Master Mix in an MX3005Pro light cycler (Agilent, Böblingen, Germany). Primer sequences were as follows: mS12 fw GAAGCTGCCAAGGCCTTAGA; mS12 rev AACTGCAACCAACCACCTTC; ArhGAP1 fw CATTGCCGGAACGAGCCAT; ArhGAP1 rev TACTTGAGCACTTGGCGAGG; ArhGAP5 fw TGGAAGCAGCAAAAATCCCAG; ArhGAP5 rev TGACAGAAATTGCCACGGGA; ArhGAP18 fw CTGGCTATCGAGTTCCTCGG; ArhGAP18 rev GGCAGTCTGAAACTGGGCAA; ArhGAP19 fw GGCTTATCAAGCGCAAAGTCC; ArhGAP19 rev CCCTCTCTCTTCGCCTCAGA; ArhGAP21 fw AAGGGCAAGAGAGTTGGTGG; ArhGAP21 rev TGGCAACTGTTCTGTTTTGCT; ArhGAP29 fw ATCTGAGGCGAGTGGTGGAT; ArhGAP29 rev AGCAGCTTGGGGCTTTTACA; ArhGAP35 fw CAAACCAAAGCCTCCTGTGC; ArhGAP35 rev TGCTTAGTCCTGTGGCTTCG; Gmip fw GCTCAGCTGGTTGAGTTCCT; Gmip rev GCCCCATCTCTGGTGTCTTC; Hmha1 fw

GAGCAATGTGGTCCAGAGACA; Hmha1 rev AATGAAAGGCTTTGACCTTGGC; Ophn1 fw TCAAAGCGCTTGCTGAGAGA; Ophn1 rev AGATGCCACCACGGATGATG; Stard13 fw TCTGTGGCTCTCTCCTGGG; Stard13 rev TGGGGAACTGCGAATCTTCA; ArhGEF1 fw CTAAAGGTCGAGGCTGATGAGA; ArhGEF1 rev CCCTGATAGCCTCTTCCACC; ArhGEF10 fw GGAGCCATGGAGATTCAGCA; ArhGEF10 rev TTGGAGAACGAGGCCACAAA; ArhGEF11 fw CTGAGATCGACCTACGCCTG; ArhGEF11 rev GGTCTTAGGGAAGAAGGGCAG; ArhGEF15 fw AAGCGGCCTCACTATCAGAC; ArhGEF15 rev CGTGGGCTCAGATGGTCTTG; ArhGEF18 fw GAACATCTGGATGGCCCACA; ArhGEF18 rev CGGTGGACCAGCTCTAATTCC; TAGLN fw TCCAGTCCACAAACGACCAA; TAGLN rev CCAATTTGCTCAGAATCACACCA, Net1 fw TTCAAATCCCCGGATGACGG; Net1 rev GGTAGGCCTTTCTAGCGAGC; Trio fw TACAGGAAGCCACGAGAAGG; Trio rev ACTCCCTGGACCTAGAACCC; ACTA2 fw GCCAGTCGCTGTCAGGAACCC; ACTA2 rev GCCAGCCAAGTCCAGACGCA; PHD3 fw GGCCGCTGTATCACCTGTAT; PHD3 rev, TTCTGCCCTTTCTTCAGCAT; CTGF fw GTGTGCACTGCCAAAGATGGT; CTGF rev GTCCGGATGCACTTTTTGCC.

mS12 was used as housekeeping gene. The fold change in gene expression was calculated by using the delta-delta CT method.

Protein extraction and immunoblot analyses

Cell lysates were generated as described previously (Vogler et al., 2013). Briefly, cells were lysed in 400 mM NaCl, 1 mM EDTA, 10 mM Tris/HCl pH 8.0, 0.1% Triton X-100, supplemented with the protease inhibitors (Roche Applied Science, Mannheim, Germany). For immunoblot analysis, protein extracts were resolved by SDS-PAGE and electro-transferred onto nitrocellulose membranes (Amersham, Freiburg, Germany) by semi-dry blotting (PeqLab, Erlangen, Germany). Primary antibodies used were: anti-HIF-1α (1:1000, NB-100-479, Novus, Littleton, USA), anti-β-tubulin (1:1000, Abcam, Cambridge, UK, ab6046), anti-ArhGAP29 (1:2000,anti-PARG1; Novus, NBP1-05989), anti-vinculin-1 (1:10000, Sigma Aldrich, V9264), anti-RhoA (1:1000, Cell Signaling Technology, Danvers, USA, 67B9 mAb #2117).

For detection of immunocomplexes, horseradish peroxidase (HRP) -conjugated secondary goat anti-rabbit (1:10000, sc2004, Santa Cruz Biotechnology, Dallas, USA) or goat anti-mouse antibodies (1:1000, sc3738, Santa Cruz Biotechnology, Dallas, USA) were used. Membranes were incubated with chemilumiescent HRP substrate (Merck Millipore, Darmstadt, Germany). Western Blots were quantified using ImageJ.

RhoA-GTP pulldown assays

RhoA activity was measured by pull-down assays modified from Ren *et al.* (Ren et al., 1999). Briefly, cells were washed twice with ice-cold PBS, then lysed in ice-cold lysis buffer (25 mM HEPES (pH 7.5), 150 mM NaCL, 10 mM $MgCl_2$, 1% NP-40, 1 mM EDTA, 10% Glycerol) supplemented with protease and phosphatase inhibitors (100 µM PMSF, 25 mM NaF, 1 mM Na_3VO_4, protease inhibitor mix tablet (Roche, Basel, Switzerland)). Cleared lysates were incubated with 100 µl GST-Rhotekin-RBD beads

for 1 h at 4°C under end-to-end rotation. Beads were washed 3 times with lysis buffer. Total cell lysates and the Rhotekin-RBD-captured proteins were analyzed by Western blotting.

Statistical analysis

Unless indicated otherwise in the figure legend, data were analyzed by unpaired 2-tailed Student´s *t* test and presented as mean ± s.e.m.. Statistical significance was calculated with GraphPad Prism 5 software. A p-value < 0.05 was considered statistically significant. The number of samples (biological replicates) analyzed in each experiment is indicated in the figure legends. If not indicated otherwise, experiments were at least repeated twice and one representative experiment is shown.

Footnotes

Competing interests

The authors declare no competing or financial interests.

Author contributions:

Conceptualization: L.L., A.J.R., S.L., D.M.K., A.Z.; Methodology: L.L., M.V., A.J.R., M.L. S.L., D.M.K., A.Z.; Validation: L.L., D.M.K., A.Z.; Formal analysis: L.L., J.P., L.H., G.J.v.B., D.M.K., A.Z.; Investigation: L.L., J.P., S.K., L.H., M.V., A.Z.; Resources. A.J.R., S.L.; Writing – original draft: D.M.K., A.Z.; Writing – review & editing: L.L., G.J.v.B, A.J.R., S.L., D.M.K., A.Z.; Visualization: D.M.K., A.Z.; Supervision: D.M.K., A.Z.; Project administration: D.K.M., A.Z.; Funding acquisition: D.K.M.

Funding:

L.L. is supported by the Deutsche Forschungsgemeinschaft (DFG)-funded GRK1816/IRTG1816. This work was also supported by Cancer Research UK #C6620/A15961 to A.J. R.

Figure Legends

Figure 1: Hypoxia suppresses the transdifferentiation of fibroblasts into myofibroblasts.

Primary skin fibroblasts were incubated in normoxia (20% O_2) and hypoxia (1% O_2) for the indicated time periods and analyzed for αSMA and TGLN expression by qRT-PCR **(A)** or by immunofluorescence analysis in combination with phalloidin staining **(B)**. In A four samples were analyzed. Arrows in B indicate positive cells, in which αSMA colocalizes with F-actin. **(C)** Quantification of αSMA-positive cells from the experiments in B. Fibroblasts isolated from three different animals were included; in each condition a total of at least 200 cells were analyzed. **(D)** Primary skin fibroblasts were stimulated with TGF-β in normoxia and hypoxia for 24 h. Subsequently, αSMA and TGLN mRNA levels were quantified by qRT-PCR. Four samples were analyzed. **(E)** Effect of hypoxia on collagen gel contraction. Cells grown in collagen gels were incubated in normoxia (20% O_2) and hypoxia (1% O_2) for 24 h. Gels were lifted and collagen areas were determined over a time period of 24 h. Representative gel images are shown. For each condition 4 collagen gels were analyzed. *$p<0.05$.

Figure 2: F-actin structures and RhoA activity are altered in hypoxia.

(A) Representative images of primary skin fibroblasts incubated for 24 h in normoxia (20% O_2) and hypoxia (1% O_2) stained for F-actin with Alexa-fluor 594 conjugated phalloidin, and corresponding pseudocolored images in which each color refers to an F-actin cluster. **(B)** F-actin cluster (c1 - c6) distribution for primary cells incubated at 20% O_2 and 1% O_2 for 24 h from at least 11 cells per condition. F-actin cluster distribution was analyzed using the MiToBo plugin for ImageJ. **(C)** Primary skin fibroblasts were incubated at 20% O_2 for 24 h with or without the addition of the Rho inhibitor C3 transferase. Subsequently, cells were analyzed by immunofluorescence and Alexa-fluor 594 conjugated phalloidin staining for αSMA and F-actin. **(D)** Quantification of positive cells, in which αSMA colocalizes with F-actin. Fibroblasts isolated from four different animals were included. In each condition a total of at least 100 cells were analyzed. In GST-RBD pulldown assays in primary fibroblasts **(E)**, L929 cells **(F)** and mouse embryonic fibroblasts (MEF) **(G)** cells show a reversible RhoA activation in hypoxia. Active, GTP-bound RhoA was sedimented from cell lysates with GST- RBD beads after normoxic (20% O_2) and hypoxic cell incubation (1% O_2, for the indicated time points). GST-RBD bound protein and total cell lysates were analyzed with the indicated antibodies in Western blots. GST-RBD bound protein and total cell lysates were analyzed by Western blotting. Tubulin was used as a loading control. *$p < 0.05$.

Figure 3: ArhGAP29 is induced under hypoxic conditions.

(A) qRT-PCR analyses of mRNAs coding for the indicated RhoA-GEFs and RhoA-GAPs were performed after 24 h of normoxic (20% O_2) and hypoxic (1% O_2) incubation of L929 cells. In each analysis at least 3 different samples were included. mRNA levels at 20% O_2 were set to 1. L929 fibroblasts were exposed to hypoxia (1% O_2) for the indicated time points. ArhGAP29 mRNA expression **(B)** and protein levels **(C)** were analyzed via qRT-PCR and Western blot analysis. mRNA levels at 20% O_2 were set to 1. L929 cells were treated with 1 mM DMOG for 24 h. Subsequently, ArhGAP29 mRNA **(D)** and protein levels **(E)** were analyzed. **(F)** The mRNA expression levels of ArhGAP29 were analyzed in cell lines (C2C12 and mouse embryonic fibroblasts, MEF), primary cardiac

fibroblasts (PCF) and primary skin fibroblasts (PSF) after normoxic (20% O_2) and hypoxic incubation (1% O_2) for 24 h. mRNA levels at 20% O_2 were set to 1. At least three samples were included in each condition. *$p < 0.05$.

Figure 4: The hypoxic induction of ArhGAP29 is HIF-1α dependent.

L929 control and shRNA control transduced cells (shC) as well as HIF-1α knockdown cell lines (c1 and c2) and MEF wild type (MEF +/+) and HIF-1α knockout MEF cells (MEF-/-) were grown in normoxia (20% O_2) or hypoxia (1% O_2) for 4 h (MEF) or 24 h (L929). Subsequently ArhGAP29 and PHD3 mRNA expression levels were analyzed by qRT-PCR **(A, B, D, E)** and ArhGAP29 as well as HIF-1α protein levels by Western blot analyses **(C** and **F)**. Vinculin was used as a loading control. For the mRNA analyses at least three samples per condition were analyzed in the qRT-PCR analyses. *$p < 0.05$.

Figure 5: Knockdown of ArhGAP29 results in elevated RhoA activity and remodeling of the actin cytoskeleton.

ArhGAP29 knockdown (ArhGAP29 kd) cell lines were established. ArhGAP29 knockdown efficiency was determined by qRT-PCR **(A)** and Western blot **(B).** Shown are bands from the same Western blot with the same exposure time. For qRT-PCR control mRNA levels at 20% O_2 were set to 1. At least three samples were included in the qRT-PCR analyses per condition. Active, GTP-bound RhoA was sedimented from cell lysates with GST-RBD beads in control and ArhGAP29 kd cells after cultivating the cells in normoxia **(C)** as well as after normoxic (20% O_2) and hypoxic cell incubation (1% O_2, for 30 min, 4 h and 24 h) (**D**). GST-RBD bound protein and total cell lysates were analyzed by the indicated antibodies in Western blot analyses. In C three independent control and ArhGAP29 kd samples were loaded onto the SDS-Gel. Please note that the Western blot exposure time used in D was different compared to Fig. 2F to prevent overexposing the kd samples.

Figure 6: ArhGAP29 knockdown results in increased Myocardin related transcription factor (MRTF) nuclear accumulation and serum response factor (SRF) signaling

Localization of endogenous MRTF-A **(A)** or overexpressed GFP-tagged MTRF-A **(C)** in control and ArhGAP29 knockdown L929 cells was analyzed by immunofluorescence after normoxic (20% O_2) and hypoxic (1% O_2, 4 h) incubation with and without addition of the Rho-inhibitor C3 transferase and quantified using ImageJ. Representative images are shown in which nuclear areas were encircled for better visibility. **(B, D)** Quantification of the experiments shown in A and C ($n \geq 36$ cells per condition). **(E)** L929 control and ArhGAP kd cells were transfected with a serum response element driven firefly luciferase (FL) and a constitutively active renilla luciferase (RL) reporter gene plasmid. Subsequently, cells were exposed to normoxia (20% O_2) or hypoxia (1% O_2) for 24 h and lysed. FL and RL activities were analyzed. In each condition at least three samples were included. **(F)** CTGF mRNA expression was analyzed via qRT-PCR in L929 control and ArhGAP29 kd cells after incubation in normoxic 20% O_2 and hypoxic condition (1% O_2) for 24 h. mRNA levels of control cells at 20% O_2 were set to 1. For each condition at least three samples were included. *$p < 0.05$.

Figure 7: Knockdown of ArhGAP29 in primary skin fibroblasts modulates the myofibroblastic differentiation

Primary fibroblasts (control), primary fibroblasts transduced with scrambled shRNA (shC) as well as ArhGAP29 knockdown (ArhGAP29 kd) primary fibroblasts were incubated in normoxia (20% O_2) and hypoxia (1% O_2). Cells were analyzed for αSMA expression by qRT-PCR **(A)** or immunofluorescence analysis. **(B)** Quantification of αSMA-positive cells. Fibroblasts isolated from six different animals were analyzed. At least 200 cells were analyzed per condition. Statistical analysis was done using paired two-tailed Student`s t-test. *$p < 0.05$. **(C)** Schematic representation of the role of ArhGAP29 for the myofibroblastic differentiation in hypoxia. In normoxia fibroblasts transdifferentiate over time into αSMA-expressing myofibroblasts. In hypoxia ArhGAP29 is induced in a HIF-1α dependent manner. The hypoxic induction of ArhGAP29 modulates RhoA activity and inhibits MRTF-A activity and thus αSMA expression. The knockdown of ArhGAP29 restores myofibroblastic cell properties in hypoxia.

References

Amin, E., Jaiswal, M., Derewenda, U., Reis, K., Nouri, K., Koessmeier, K.T., Aspenstrom, P., Somlyo, A.V., Dvorsky, R., and Ahmadian, M.R. (2016). Deciphering the Molecular and Functional Basis of RHOGAP Family Proteins: A SYSTEMATIC APPROACH TOWARD SELECTIVE INACTIVATION OF RHO FAMILY PROTEINS. *The Journal of biological chemistry* **291**, 20353-20371.

Bailly, K., Ridley, A.J., Hall, S.M., and Haworth, S.G. (2004). RhoA activation by hypoxia in pulmonary arterial smooth muscle cells is age and site specific. *Circulation research* **94**, 1383-1391.

Barry, D.M., Koo, Y., Norden, P.R., Wylie, L.A., Xu, K., Wichaidit, C., Azizoglu, D.B., Zheng, Y., Cobb, M.H., Davis, G.E.*, et al.* (2016). Rasip1-Mediated Rho GTPase Signaling Regulates Blood Vessel Tubulogenesis via Nonmuscle Myosin II. *Circulation research* **119**, 810-826.

Bishop, T., and Ratcliffe, P.J. (2014). Signaling hypoxia by hypoxia-inducible factor protein hydroxylases: a historical overview and future perspectives. *Hypoxia* **2**, 197-213.

Bochaton-Piallat, M.L., Gabbiani, G., and Hinz, B. (2016). The myofibroblast in wound healing and fibrosis: answered and unanswered questions. *F1000Research* **5**.

Botusan, I.R., Sunkari, V.G., Savu, O., Catrina, A.I., Grunler, J., Lindberg, S., Pereira, T., Yla-Herttuala, S., Poellinger, L., Brismar, K.*, et al.* (2008). Stabilization of HIF-1alpha is critical to improve wound healing in diabetic mice. *Proceedings of the National Academy of Sciences of the United States of America* **105**, 19426-19431.

Butali, A., Mossey, P., Adeyemo, W., Eshete, M., Gaines, L., Braimah, R., Aregbesola, B., Rigdon, J., Emeka, C., Olutayo, J.*, et al.* (2014). Rare functional variants in genome-wide association identified candidate genes for nonsyndromic clefts in the African population. *American journal of medical genetics Part A* **164A**, 2567-2571.

Chandrasekharan, D., and Ramanathan, A. (2014). Identification of a novel heterozygous truncation mutation in exon 1 of ARHGAP29 in an Indian subject with nonsyndromic cleft lip with cleft palate. *European journal of dentistry* **8**, 528-532.

Dang, C.V., Reddy, E.P., Shokat, K.M., and Soucek, L. (2017). Drugging the 'undruggable' cancer targets. *Nature reviews Cancer* **17**, 502-508.

Epstein, A.C., Gleadle, J.M., McNeill, L.A., Hewitson, K.S., O'Rourke, J., Mole, D.R., Mukherji, M., Metzen, E., Wilson, M.I., Dhanda, A.*, et al.* (2001). C. elegans EGL-9 and mammalian homologs define a family of dioxygenases that regulate HIF by prolyl hydroxylation. *Cell* **107**, 43-54.

Fediuk, J., Gutsol, A., Nolette, N., and Dakshinamurti, S. (2012). Thromboxane-induced actin polymerization in hypoxic pulmonary artery is independent of Rho. *American journal of physiology Lung cellular and molecular physiology* **302**, L13-26.

Gilkes, D.M., Xiang, L., Lee, S.J., Chaturvedi, P., Hubbi, M.E., Wirtz, D., and Semenza, G.L. (2014). Hypoxia-inducible factors mediate coordinated RhoA-ROCK1 expression and signaling in breast cancer cells. *Proceedings of the National Academy of Sciences of the United States of America* **111**, E384-393.

Goffin, J.M., Pittet, P., Csucs, G., Lussi, J.W., Meister, J.J., and Hinz, B. (2006). Focal adhesion size controls tension-dependent recruitment of alpha-smooth muscle actin to stress fibers. *J Cell Biol* **172**, 259-268.

Gonzalez-Rodriguez, P., Falcon, D., Castro, M.J., Urena, J., Lopez-Barneo, J., and Castellano, A. (2015). Hypoxic induction of T-type Ca(2+) channels in rat cardiac myocytes: role of HIF-1alpha and RhoA/ROCK signalling. *The Journal of physiology* **593**, 4729-4745.

Hall, A. (2005). Rho GTPases and the control of cell behaviour. *Biochemical Society transactions* **33**, 891-895.

Hinz, B., Gabbiani, G., and Chaponnier, C. (2002). The NH2-terminal peptide of alpha-smooth muscle actin inhibits force generation by the myofibroblast in vitro and in vivo. *J Cell Biol* **157**, 657-663.

Hinz, B., Phan, S.H., Thannickal, V.J., Prunotto, M., Desmouliere, A., Varga, J., De Wever, O., Mareel, M., and Gabbiani, G. (2012). Recent developments in myofibroblast biology: paradigms for connective tissue remodeling. *The American journal of pathology* **180**, 1340-1355.

Hodge, R.G., and Ridley, A.J. (2016). Regulating Rho GTPases and their regulators. *Nature reviews Molecular cell biology* **17**, 496-510.

Hong, W.X., Hu, M.S., Esquivel, M., Liang, G.Y., Rennert, R.C., McArdle, A., Paik, K.J., Duscher, D., Gurtner, G.C., Lorenz, H.P.*, et al.* (2014). The Role of Hypoxia-Inducible Factor in Wound Healing. *Advances in wound care* **3**, 390-399.

Ivan, M., Kondo, K., Yang, H., Kim, W., Valiando, J., Ohh, M., Salic, A., Asara, J.M., Lane, W.S., and Kaelin, W.G., Jr. (2001). HIFalpha targeted for VHL-mediated destruction by proline hydroxylation: implications for O2 sensing. *Science* **292**, 464-468.

Jaakkola, P., Mole, D.R., Tian, Y.M., Wilson, M.I., Gielbert, J., Gaskell, S.J., von Kriegsheim, A., Hebestreit, H.F., Mukherji, M., Schofield, C.J.*, et al.* (2001). Targeting of HIF-alpha to the von Hippel-Lindau ubiquitylation complex by O2-regulated prolyl hydroxylation. *Science* **292**, 468-472.

Jun, J.I., and Lau, L.F. (2018). Resolution of organ fibrosis. *The Journal of clinical investigation* **128**, 97-107.

Katschinski, D.M. (2009). In vivo functions of the prolyl-4-hydroxylase domain oxygen sensors: direct route to the treatment of anaemia and the protection of ischaemic tissues. *Acta physiologica* **195**, 407-414.

Kimura, K., Iwano, M., Higgins, D.F., Yamaguchi, Y., Nakatani, K., Harada, K., Kubo, A., Akai, Y., Rankin, E.B., Neilson, E.G.*, et al.* (2008). Stable expression of HIF-1alpha in tubular epithelial cells promotes interstitial fibrosis. *American journal of physiology Renal physiology* **295**, F1023-1029.

Kis, K., Liu, X., and Hagood, J.S. (2011). Myofibroblast differentiation and survival in fibrotic disease. *Expert Rev Mol Med* **13**, e27.

Leslie, E.J., Carlson, J.C., Shaffer, J.R., Feingold, E., Wehby, G., Laurie, C.A., Jain, D., Laurie, C.C., Doheny, K.F., McHenry, T.*, et al.* (2016). A multi-ethnic genome-wide association study identifies novel loci for non-syndromic cleft lip with or without cleft palate on 2p24.2, 17q23 and 19q13. *Human molecular genetics* **25**, 2862-2872.

Liu, H., Busch, T., Eliason, S., Anand, D., Bullard, S., Gowans, L.J.J., Nidey, N., Petrin, A., Augustine-Akpan, E.A., Saadi, I.*, et al.* (2017a). Exome sequencing provides additional evidence for the involvement of ARHGAP29 in Mendelian orofacial clefting and extends the phenotypic spectrum to isolated cleft palate. *Birth defects research* **109**, 27-37.

Liu, H., Leslie, E.J., Carlson, J.C., Beaty, T.H., Marazita, M.L., Lidral, A.C., and Cornell, R.A. (2017b). Identification of common non-coding variants at 1p22 that are functional for non-syndromic orofacial clefting. *Nature communications* **8**, 14759.

Madsen, C.D., Pedersen, J.T., Venning, F.A., Singh, L.B., Moeendarbary, E., Charras, G., Cox, T.R., Sahai, E., and Erler, J.T. (2015). Hypoxia and loss of PHD2 inactivate stromal fibroblasts to decrease tumour stiffness and metastasis. *EMBO reports* **16**, 1394-1408.

Mao, J., Yuan, H., Xie, W., and Wu, D. (1998). Guanine nucleotide exchange factor GEF115 specifically mediates activation of Rho and serum response factor by the G protein alpha subunit Galpha13. *Proceedings of the National Academy of Sciences of the United States of America* **95**, 12973-12976.

Marxsen, J.H., Stengel, P., Doege, K., Heikkinen, P., Jokilehto, T., Wagner, T., Jelkmann, W., Jaakkola, P., and Metzen, E. (2004). Hypoxia-inducible factor-1 (HIF-1) promotes its degradation by induction of HIF-alpha-prolyl-4-hydroxylases. *Biochem J* **381**, 761-767.

Modarressi, A., Pietramaggiori, G., Godbout, C., Vigato, E., Pittet, B., and Hinz, B. (2010). Hypoxia impairs skin myofibroblast differentiation and function. *The Journal of investigative dermatology* **130**, 2818-2827.

Möller, B., Glaß, M., Misiak, D., and Posch, S. (2016). MiToBo - A Toolbox for Image Processing and Analysis. Journal of Open Research Software. *Journal of open research software* **4e17**.

O'Connor, K., and Chen, M. (2013). Dynamic functions of RhoA in tumor cell migration and invasion. *Small GTPases* **4**, 141-147.

Olson, E.N., and Nordheim, A. (2010). Linking actin dynamics and gene transcription to drive cellular motile functions. *Nature reviews Molecular cell biology* **11**, 353-365.

Post, A., Pannekoek, W.J., Ross, S.H., Verlaan, I., Brouwer, P.M., and Bos, J.L. (2013). Rasip1 mediates Rap1 regulation of Rho in endothelial barrier function through ArhGAP29. *Proceedings of the National Academy of Sciences of the United States of America* **110**, 11427-11432.

Qiao, Y., Chen, J., Lim, Y.B., Finch-Edmondson, M.L., Seshachalam, V.P., Qin, L., Jiang, T., Low, B.C., Singh, H., Lim, C.T.*, et al.* (2017). YAP Regulates Actin Dynamics through ARHGAP29 and Promotes Metastasis. *Cell reports* **19**, 1495-1502.

Raheja, L.F., Genetos, D.C., Wong, A., and Yellowley, C.E. (2011). Hypoxic regulation of mesenchymal stem cell migration: the role of RhoA and HIF-1alpha. *Cell biology international* **35**, 981-989.

Ren, X.D., Kiosses, W.B., and Schwartz, M.A. (1999). Regulation of the small GTP-binding protein Rho by cell adhesion and the cytoskeleton. *The EMBO journal* **18**, 578-585.

Ridley, A.J. (2006). Rho GTPases and actin dynamics in membrane protrusions and vesicle trafficking. *Trends in cell biology* **16**, 522-529.

Rossman, K.L., Der, C.J., and Sondek, J. (2005). GEF means go: turning on RHO GTPases with guanine nucleotide-exchange factors. *Nature reviews Molecular cell biology* **6**, 167-180.

Ryan, H.E., Poloni, M., McNulty, W., Elson, D., Gassmann, M., Arbeit, J.M., and Johnson, R.S. (2000). Hypoxia-inducible factor-1alpha is a positive factor in solid tumor growth. *Cancer research* **60**, 4010-4015.

Savastano, C.P., Brito, L.A., Faria, A.C., Seto-Salvia, N., Peskett, E., Musso, C.M., Alvizi, L., Ezquina, S.A., James, C., Gosgene*, et al.* (2017). Impact of rare variants in ARHGAP29 to the etiology of oral clefts: role of loss-of-function vs missense variants. *Clinical genetics* **91**, 683-689.

Scheid, A., Wenger, R.H., Schaffer, L., Camenisch, I., Distler, O., Ferenc, A., Cristina, H., Ryan, H.E., Johnson, R.S., Wagner, K.F.*, et al.* (2002). Physiologically low oxygen concentrations in fetal skin regulate hypoxia-inducible factor 1 and transforming growth factor-beta3. *FASEB journal : official publication of the Federation of American Societies for Experimental Biology* **16**, 411-413.

Sen, C.K., and Roy, S. (2010). Oxygenation state as a driver of myofibroblast differentiation and wound contraction: hypoxia impairs wound closure. *The Journal of investigative dermatology* **130**, 2701-2703.

Small, E.M. (2012). The actin-MRTF-SRF gene regulatory axis and myofibroblast differentiation. *Journal of cardiovascular translational research* **5**, 794-804.

Small, E.M., Thatcher, J.E., Sutherland, L.B., Kinoshita, H., Gerard, R.D., Richardson, J.A., Dimaio, J.M., Sadek, H., Kuwahara, K., and Olson, E.N. (2010). Myocardin-related transcription factor-a controls myofibroblast activation and fibrosis in response to myocardial infarction. *Circulation research* **107**, 294-304.

Tomasek, J.J., Gabbiani, G., Hinz, B., Chaponnier, C., and Brown, R.A. (2002a). Myofibroblasts and mechano-regulation of connective tissue remodelling. *Nature reviews Molecular cell biology* **3**, 349-363.

Tomasek, J.J., Gabbiani, G., Hinz, B., Chaponnier, C., and Brown, R.A. (2002b). Myofibroblasts and mechano-regulation of connective tissue remodelling. *Nature reviews Molecular cell biology* **3**, 349-363.

Velasquez, L.S., Sutherland, L.B., Liu, Z., Grinnell, F., Kamm, K.E., Schneider, J.W., Olson, E.N., and Small, E.M. (2013). Activation of MRTF-A-dependent gene expression with a small molecule promotes myofibroblast differentiation and wound healing. *Proceedings of the National Academy of Sciences of the United States of America* **110**, 16850-16855.

Vogelsgesang, M., Pautsch, A., and Aktories, K. (2007). C3 exoenzymes, novel insights into structure and action of Rho-ADP-ribosylating toxins. *Naunyn Schmiedebergs Arch Pharmacol* **374**, 347-360.

Vogler, M., Vogel, S., Krull, S., Farhat, K., Leisering, P., Lutz, S., Wuertz, C.M., Katschinski, D.M., and Zieseniss, A. (2013). Hypoxia modulates fibroblastic architecture, adhesion and migration: a role for HIF-1alpha in cofilin regulation and cytoplasmic actin distribution. *PloS one* **8**, e69128.

Wojciak-Stothard, B., Tsang, L.Y., and Haworth, S.G. (2005). Rac and Rho play opposing roles in the regulation of hypoxia/reoxygenation-induced permeability changes in pulmonary artery endothelial cells. *American journal of physiology Lung cellular and molecular physiology* **288**, L749-760.

Wottawa, M., Leisering, P., Ahlen, M., Schnelle, M., Vogel, S., Malz, C., Bordoli, M.R., Camenisch, G., Hesse, A., Napp, J.*, et al.* (2013). Knockdown of prolyl-4-hydroxylase domain 2 inhibits tumor growth of human breast cancer MDA-MB-231 cells by affecting TGF-beta1 processing. *International journal of cancer* **132**, 2787-2798.

Wynn, T.A. (2008). Cellular and molecular mechanisms of fibrosis. *The Journal of pathology* **214**, 199-210.

Wynn, T.A., and Ramalingam, T.R. (2012). Mechanisms of fibrosis: therapeutic translation for fibrotic disease. *Nature medicine* **18**, 1028-1040.

Xiong, A., and Liu, Y. (2017). Targeting Hypoxia Inducible Factors-1alpha As a Novel Therapy in Fibrosis. *Frontiers in pharmacology* **8**, 326.

Xu, Q., Duan, H., Gan, L., Liu, X., Chen, F., Shen, X., Tang, Y.Q., and Wang, S. (2017). MicroRNA-1291 promotes endometrial fibrosis by regulating the ArhGAP29-RhoA/ROCK1 signaling pathway in a murine model. *Mol Med Rep* **16**, 4501-4510.

Yang, M.H., Wu, M.Z., Chiou, S.H., Chen, P.M., Chang, S.Y., Liu, C.J., Teng, S.C., and Wu, K.J. (2008). Direct regulation of TWIST by HIF-1alpha promotes metastasis. *Nature cell biology* **10**, 295-305.

Zieseniss, A. (2014). Hypoxia and the modulation of the actin cytoskeleton - emerging interrelations. *Hypoxia (Auckl)* **2**, 11-21.

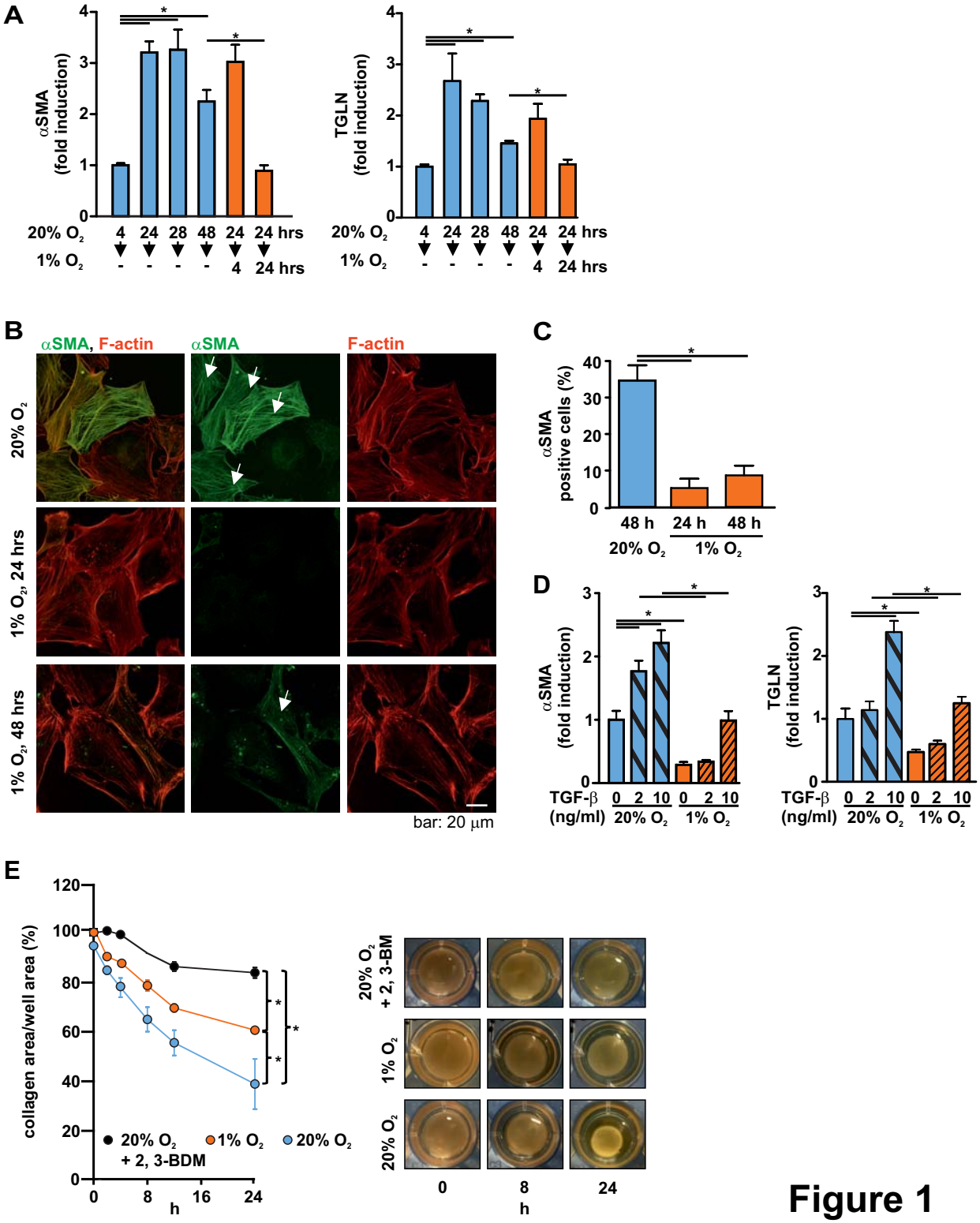
A
αSMA (fold induction)
TGLN (fold induction)
20% O2
1% O2
4 24 28 48 24 24 hrs
- - - - 4 24 hrs
B
αSMA, F-actin
αSMA
F-actin
20% O2
1% O2, 24 hrs
1% O2, 48 hrs
bar: 20 μm
C
αSMA positive cells (%)
48 h 24 h 48 h
20% O2 1% O2
D
αSMA (fold induction)
TGLN (fold induction)
TGF-β (ng/ml)
0 2 10 0 2 10
20% O2 1% O2
E
collagen area/well area (%)
20% O2
1% O2
20% O2 + 2, 3-BDM
+ 2, 3-BDM
h
0 8 24

Figure 1

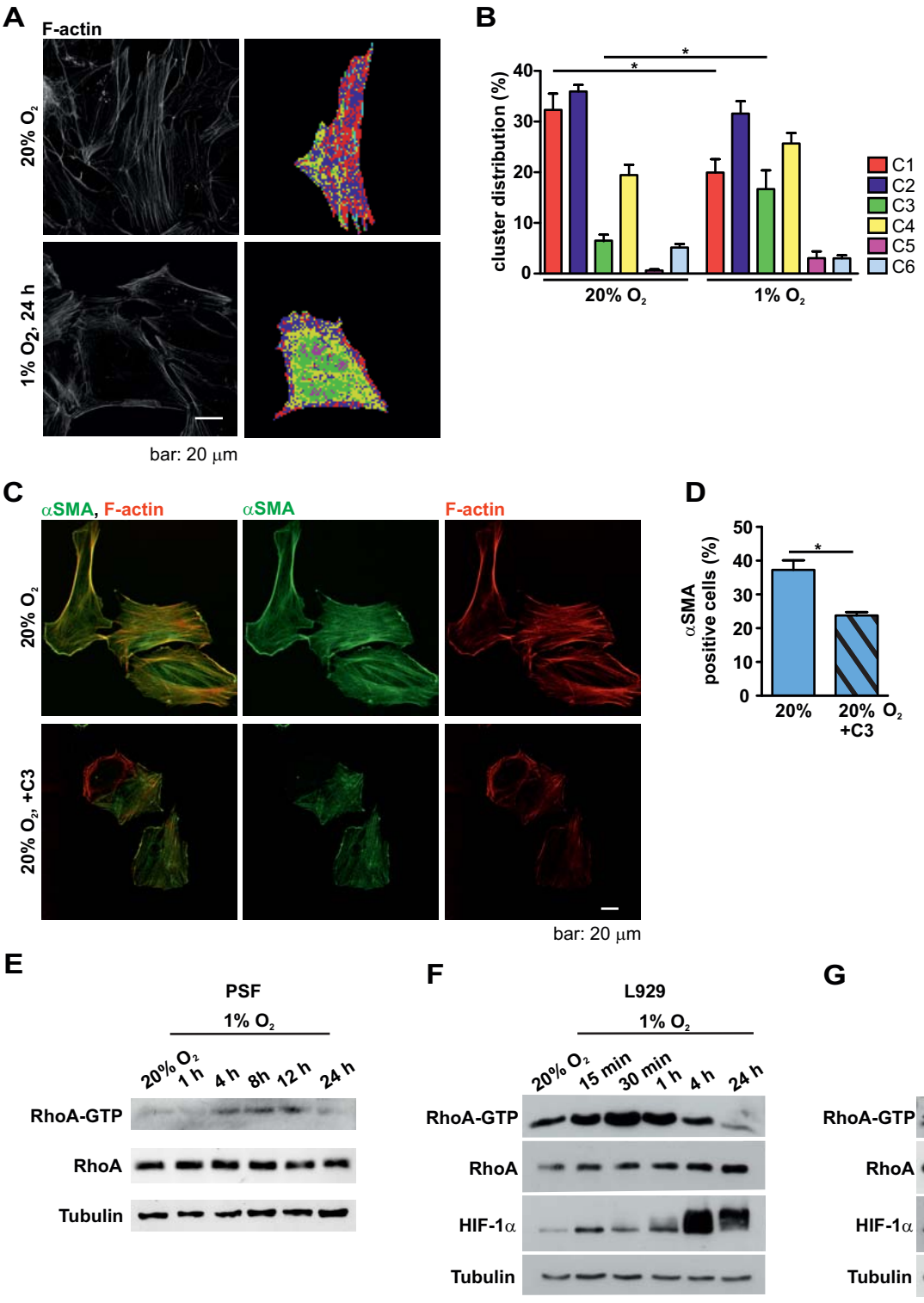
A
F-actin
20% O2
1% O2, 24 h
bar: 20 μm
B
cluster distribution (%)
40
30
20
10
0
*
*
C1
C2
C3
C4
C5
C6
20% O2
1% O2
C
αSMA, F-actin
αSMA
F-actin
20% O2
20% O2, +C3
bar: 20 μm
D
αSMA positive cells (%)
50
40
30
20
10
0
*
20%
20% O2 +C3
E
PSF
1% O2
20% O2
1 h
4 h
8h
12 h
24 h
RhoA-GTP
RhoA
Tubulin
F
L929
1% O2
20% O2
15 min
30 min
1 h
4 h
24 h
RhoA-GTP
RhoA
HIF-1α
Tubulin
G
MEF
1% O2
20% O2
15 min
30 min
1 h
4 h
24 h
RhoA-GTP
RhoA
HIF-1α
Tubulin

Figure 2

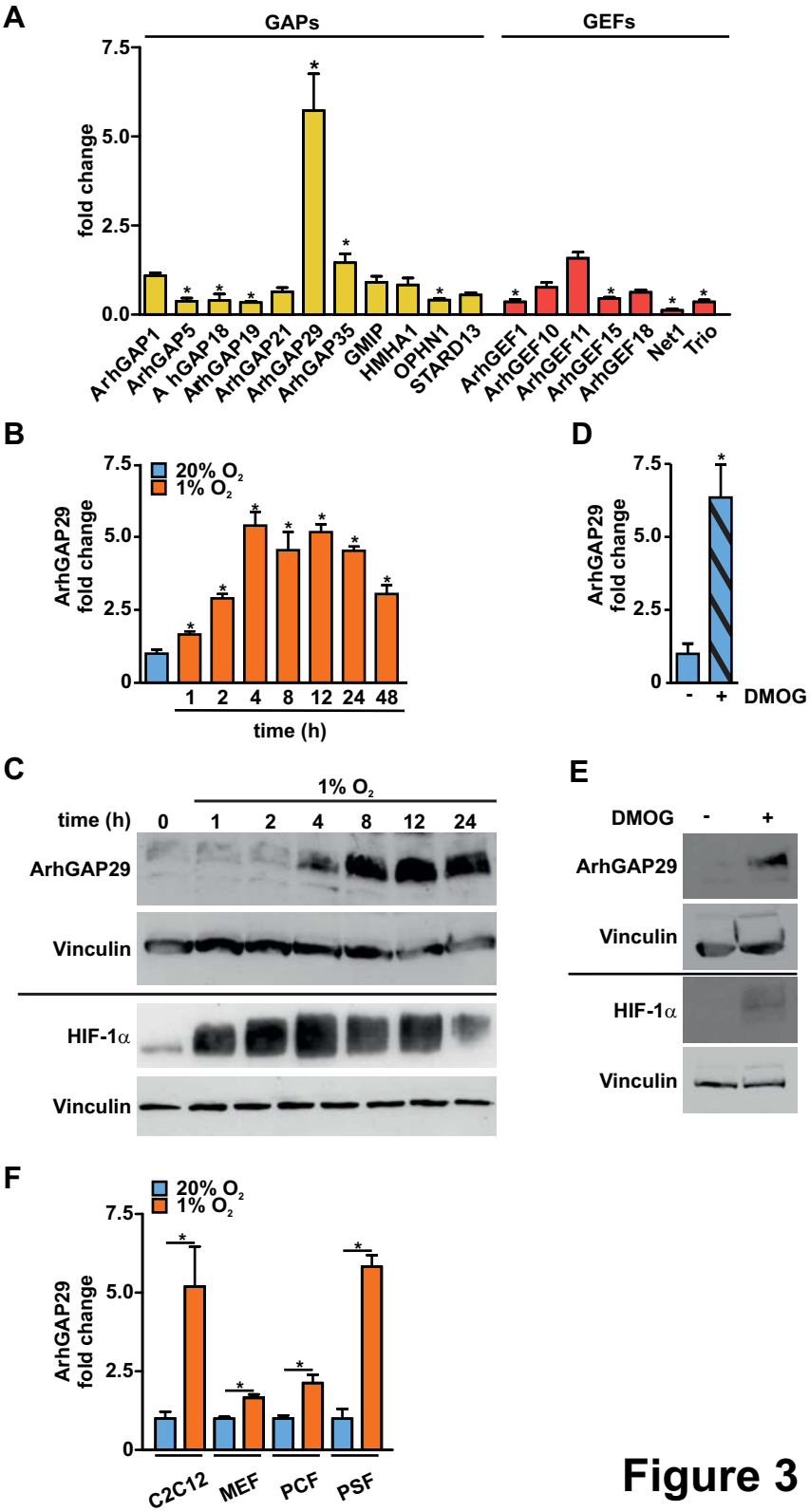
A
GAPs
GEFs
fold change
7.5
5.0
2.5
0.0
ArhGAP1
ArhGAP5
A hGAP18
ArhGAP19
ArhGAP21
ArhGAP29
ArhGAP35
GMIP
HMHA1
OPHN1
STARD13
ArhGEF1
ArhGEF10
ArhGEF11
ArhGEF15
ArhGEF18
Net1
Trio
B
20% O2
1% O2
ArhGAP29 fold change
time (h)
1 2 4 8 12 24 48
D
ArhGAP29 fold change
DMOG
C
1% O2
time (h) 0 1 2 4 8 12 24
ArhGAP29
Vinculin
HIF-1α
Vinculin
E
DMOG - +
ArhGAP29
Vinculin
HIF-1α
Vinculin
F
20% O2
1% O2
ArhGAP29 fold change
C2C12
MEF
PCF
PSF

Figure 3

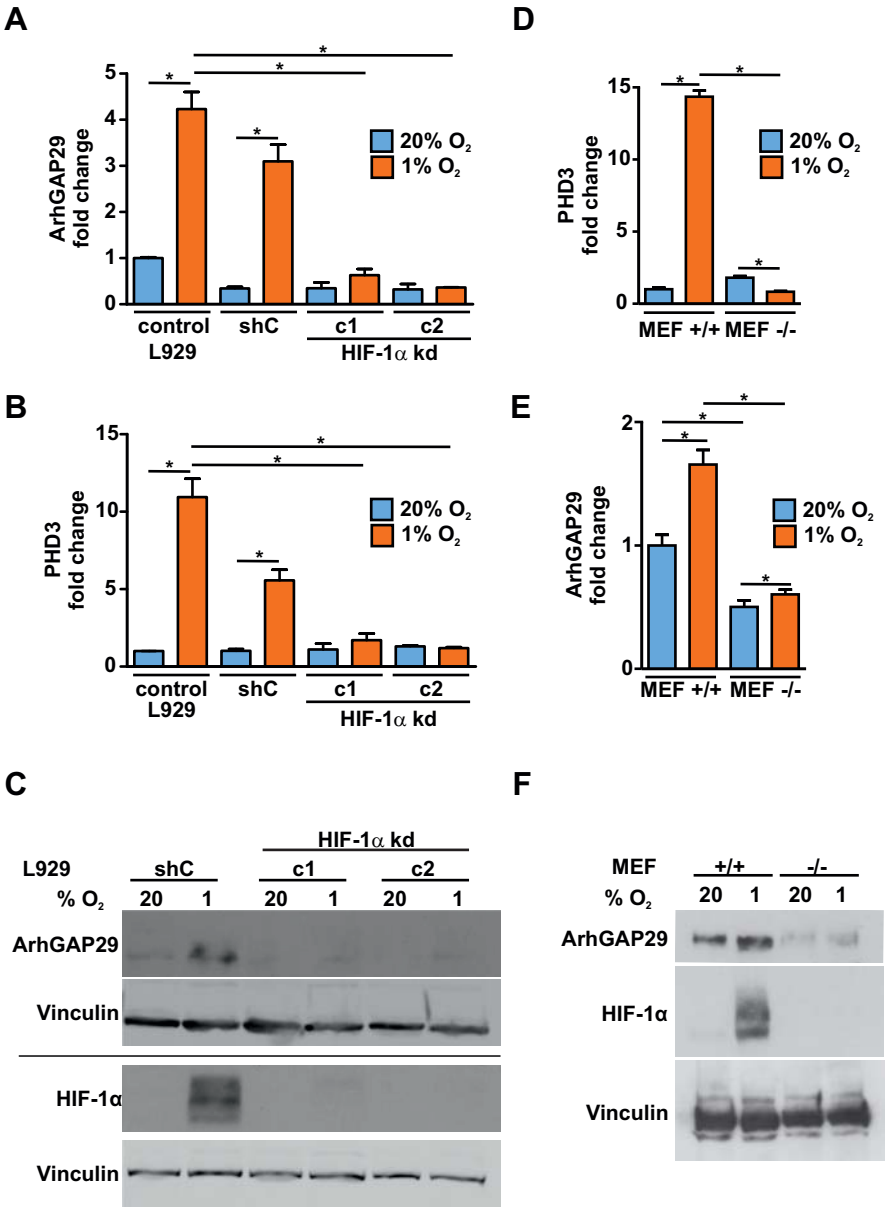
A
ArhGAP29 fold change
20% O2
1% O2
control L929
shC
c1
c2
HIF-1α kd
B
PHD3 fold change
C
L929
shC
HIF-1α kd
c1
c2
% O2
20
1
ArhGAP29
Vinculin
HIF-1α
D
MEF +/+
MEF -/-
E
F
MEF
+/+
-/-

Figure 4

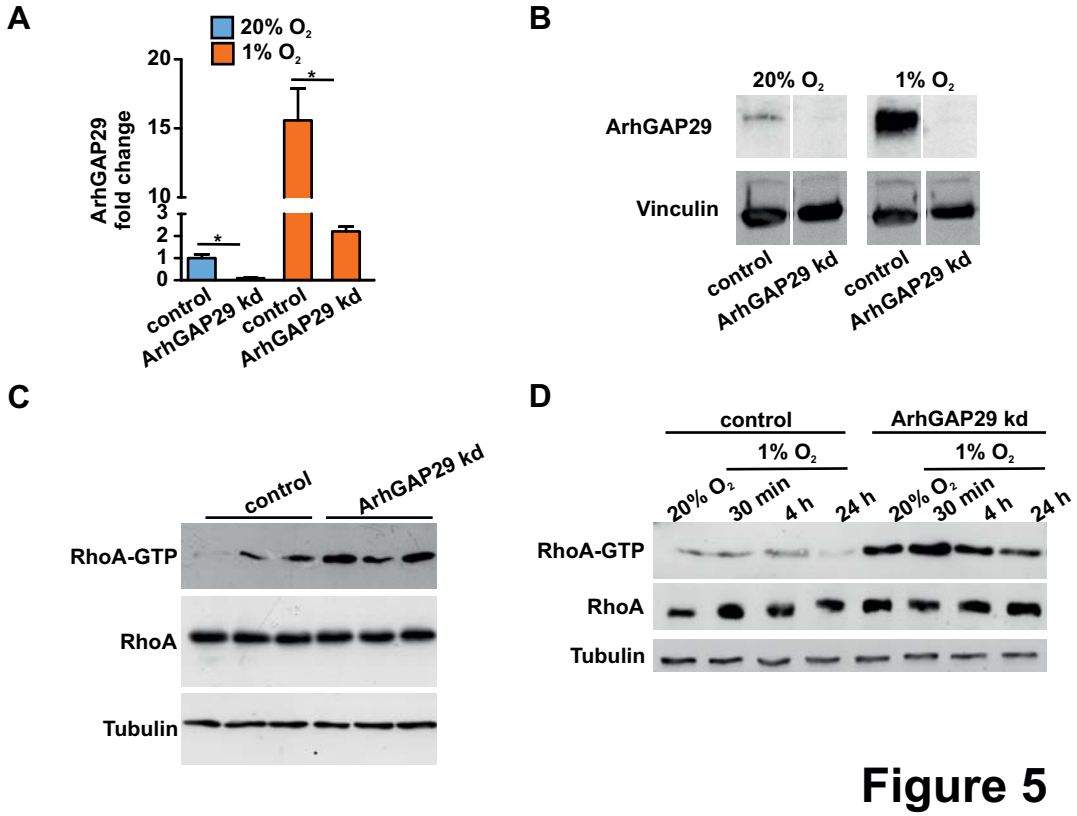
A
20% O2
1% O2
ArhGAP29 fold change
20
15
10
3
2
1
0
*
*
control
ArhGAP29 kd
control
ArhGAP29 kd
B
20% O2
1% O2
ArhGAP29
Vinculin
control
ArhGAP29 kd
control
ArhGAP29 kd
C
control
ArhGAP29 kd
RhoA-GTP
RhoA
Tubulin
D
control
ArhGAP29 kd
1% O2
1% O2
20% O2
30 min
4 h
24 h
20% O2
30 min
4 h
24 h
RhoA-GTP
RhoA
Tubulin

Figure 5

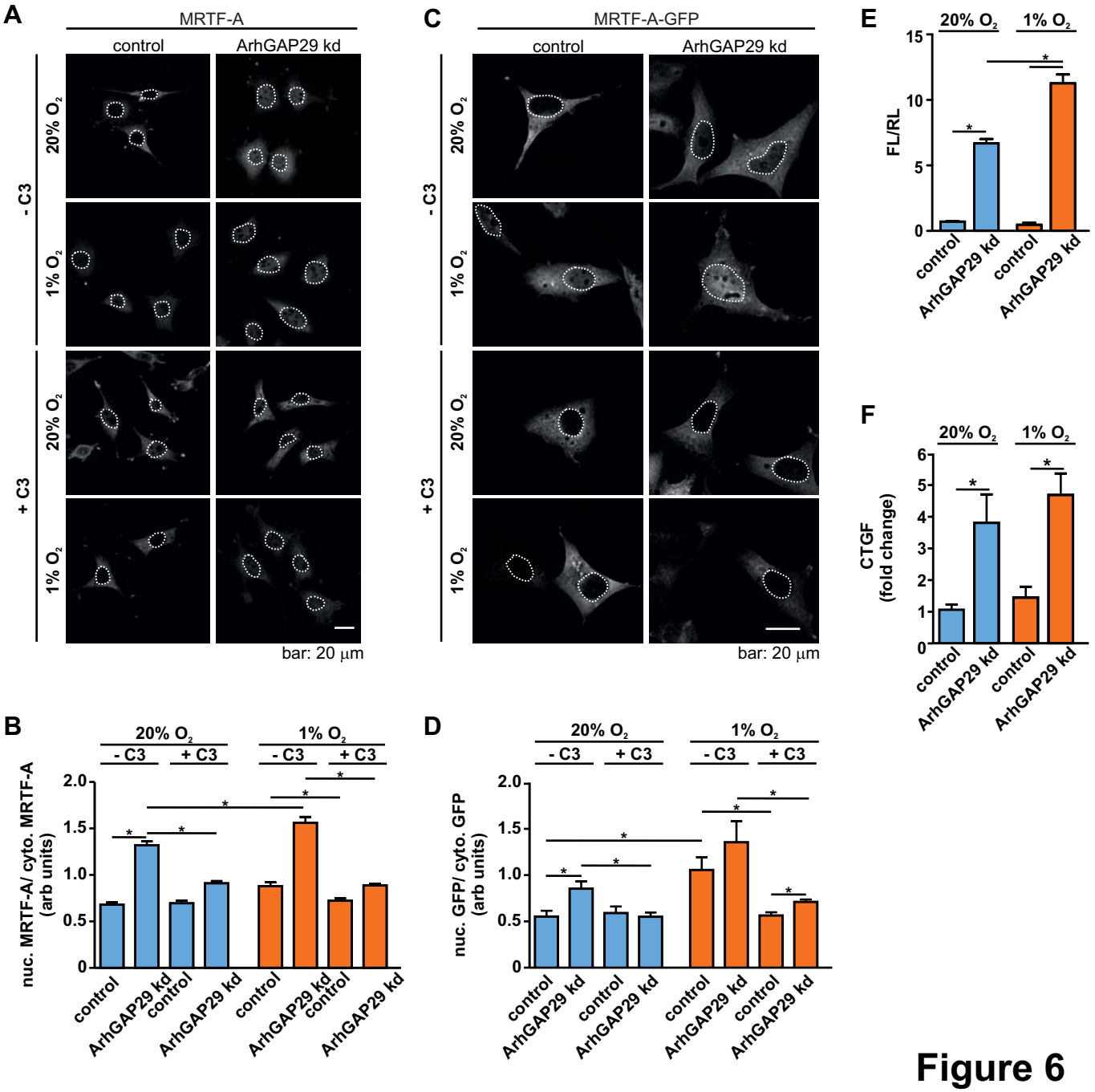
A
MRTF-A
control
ArhGAP29 kd
- C3
+ C3
20% O2
1% O2
bar: 20 μm
C
MRTF-A-GFP
control
ArhGAP29 kd
- C3
+ C3
20% O2
1% O2
bar: 20 μm
E
20% O2
1% O2
FL/RL
control
ArhGAP29 kd
control
ArhGAP29 kd
F
20% O2
1% O2
CTGF
(fold change)
control
ArhGAP29 kd
control
ArhGAP29 kd
B
20% O2
1% O2
- C3
+ C3
- C3
+ C3
nuc. MRTF-A/ cyto. MRTF-A
(arb units)
control
ArhGAP29 kd
control
ArhGAP29 kd
control
ArhGAP29 kd
control
ArhGAP29 kd
D
20% O2
1% O2
- C3
+ C3
- C3
+ C3
nuc. GFP/ cyto. GFP
(arb units)
control
ArhGAP29 kd
control
ArhGAP29 kd
control
ArhGAP29 kd
control
ArhGAP29 kd

Figure 6

Figure 7

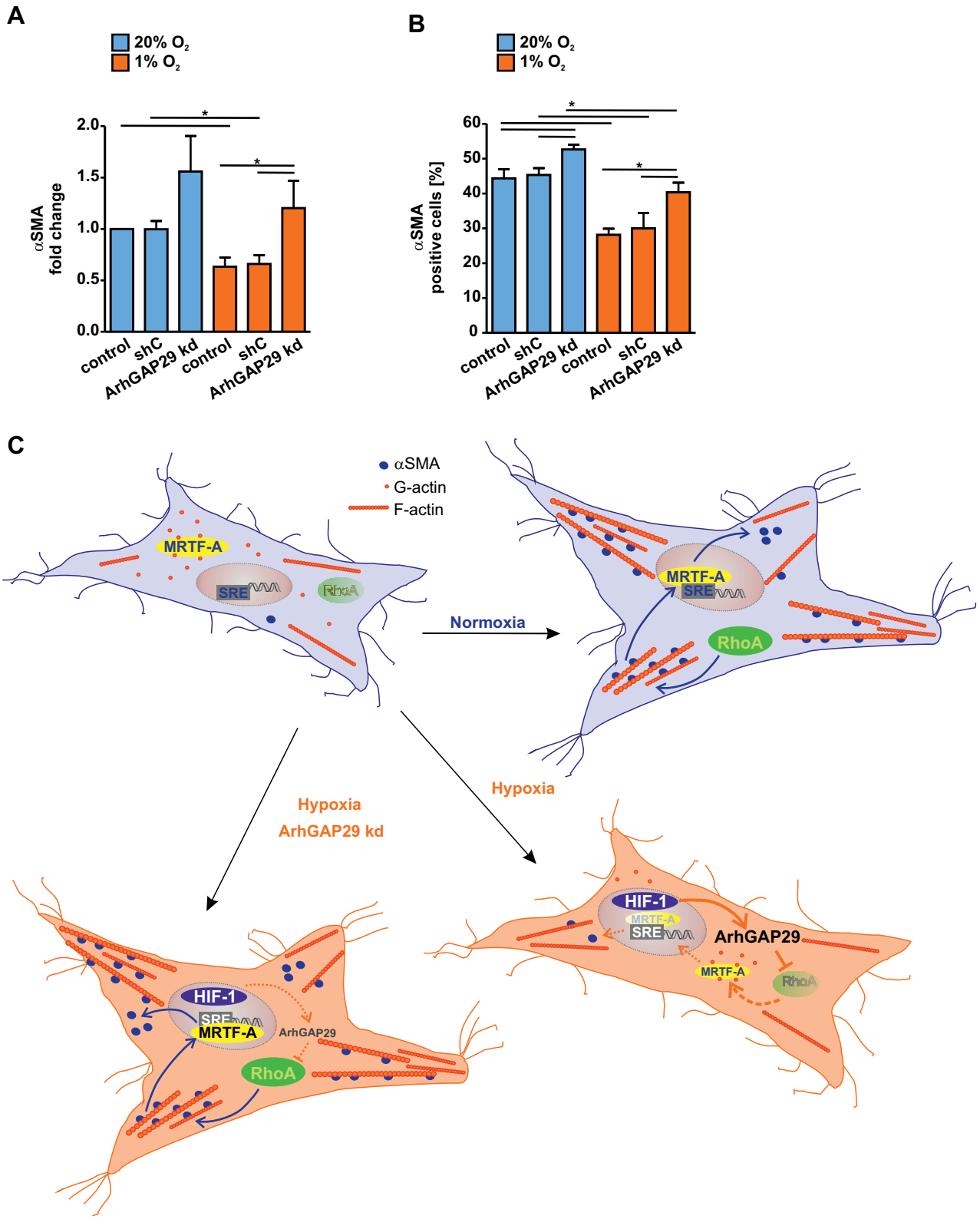
A
20% O2
1% O2
αSMA fold change
2.0
1.5
1.0
0.5
0.0
*
*
control
shC
ArhGAP29 kd
control
shC
ArhGAP29 kd
B
20% O2
1% O2
αSMA positive cells [%]
60
50
40
30
20
10
0
*
*
control
shC
ArhGAP29 kd
control
shC
ArhGAP29 kd
C
αSMA
G-actin
F-actin
MRTF-A
SRE
RhoA
Normoxia
MRTF-A
SRE
RhoA
Hypoxia
ArhGAP29 kd
Hypoxia
HIF-1
SRE
MRTF-A
ArhGAP29
RhoA
HIF-1
MRTF-A
SRE
ArhGAP29
MRTF-A
RhoA

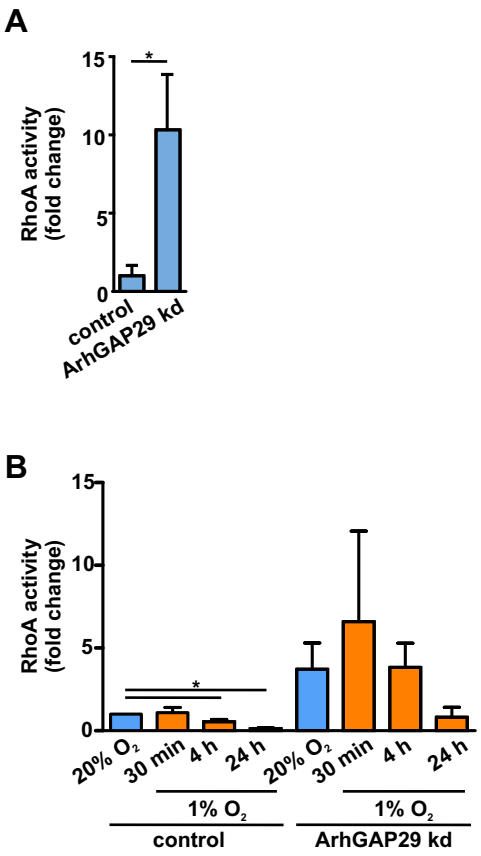
A
RhoA activity
(fold change)
15
10
5
0
*
control
ArhGAP29 kd
B
RhoA activity
(fold change)
15
10
5
0
*
20% O2
30 min
4 h
24 h
20% O2
30 min
4 h
24 h
1% O2
1% O2
control
ArhGAP29 kd

Fig. S1

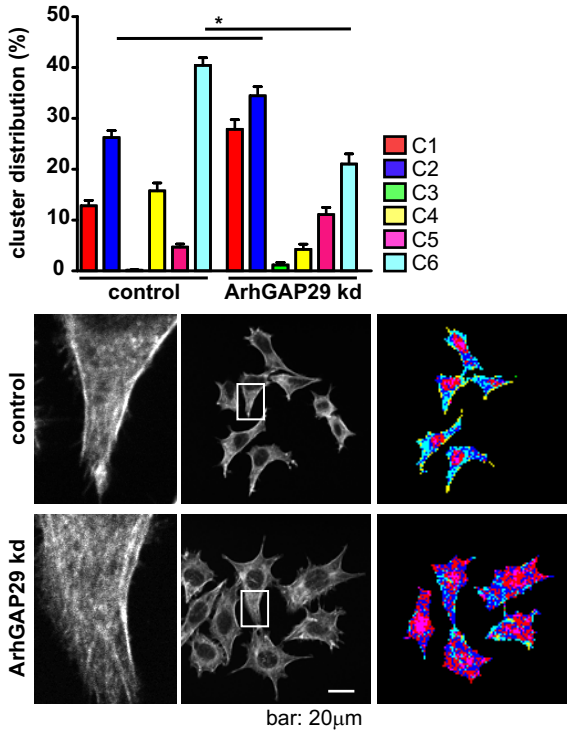
cluster distribution (%)
50
40
30
20
10
0
*
control
ArhGAP29 kd
C1
C2
C3
C4
C5
C6
control
ArhGAP29 kd
bar: 20μm

Fig. S2

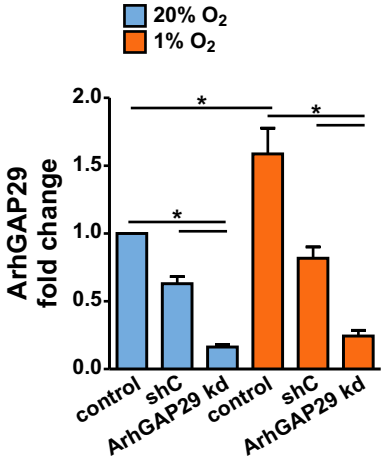
20% O2
1% O2
ArhGAP29 fold change
2.0
1.5
1.0
0.5
0.0
*
*
*
control
shC
ArhGAP29 kd
control
shC
ArhGAP29 kd

Fig. S3

Figure Legends Supplementary Figures

Supplemental Figure 1: Quantification of RhoA activity

(A) Quantification of active RhoA in control and ArhGAP29 knockdown (ArhGAP29 kd) cells in normoxia (20% O_2) shown in Fig. 6C. **(B)** Quantification of active RhoA in control and ArhGAP29 kd cells in normoxia and hypoxia. Representative experiment is shown in Fig. 5D. Four independent experiments were analyzed. Intensities of the bands were quantified with ImageJ and the precipitated active (GTP-bound) form of RhoA was normalized to the amount of total RhoA. Values are expressed as fold change compared to the control sample in normoxia. Data were analyzed by paired, two-tailed Student´s t-test. *$p < 0.05$.

Supplemental Figure 2: The knockdown of ArhGAP29 results in remodeling of the actin cytoskeleton.

Control and ArhGAP29 knockdown (kd) L929 cells were fixed and stained for F-actin. F-actin cluster distribution (c1-c6) from at least 50 cells was analyzed using the MiToBo plugin for ImageJ.

Supplemental Figure 3: Confirmation of ArhGAP29 knockdown in primary skin fibroblasts

Primary fibroblasts (control), primary fibroblasts transduced with scrambled shRNA (shC) as well as ArhGAP29 knockdown (ArhGAP29 kd) primary fibroblasts were incubated in normoxia (20% O_2) and hypoxia (1% O_2). The knockdown was confirmed via qRT-PCR. Fibroblasts isolated from six different animals were analyzed. Statistical analysis was done using paired two-tailed Student`s t-test. *$p < 0.05$.